Membrane and Water Treatment, *Vol. 16, No. 1 (2025) 1-12*
https://doi.org/10.12989/mwt.2025.16.1.001

A comparative study of membrane properties modeling used in vacuum membrane distillation theoretical studies

Nizar Loussif*[1,2] and Jamel Orfi[3]

[1]*Laboratory for the Study of Thermal and Energy Systems LESTE-LR99ES31, ENIM, University of Monastir, Monastir, 5019, Tunisia*
[2]*Higher School of Sciences and Technology of Hammam Sousse (ESSTHS), Department of Physics, University of Sousse, Sousse, 4011, Tunisia*
[3]*Mechanical Engineering Department, College of Engineering, King Saud University, P.O.Box 800, Riyadh 11421, Saudi Arabia*

(Received February 8, 2024, Revised September 21, 2024, Accepted September 23, 2024)

Abstract. In this study, a theoretical model for the transport phenomena in a vacuum membrane distillation (VMD) unit used for desalination was developed. The model is based on the conservation equations for the mass, momentum, energy and species within the feed saline solution with coupled boundary conditions, as well as on the mass and energy balances on the membrane sides. The slip velocity and temperature jump boundary conditions due to the membrane's hydrophobicity were also taken into consideration. All combinations of effective thermal conductivity and tortuosity models, usually used in membrane distillation modeling are studied and discussed to show their adequacy with experimental data from the literature for PVDF, PTFE, and PP hydrophobic membranes used in VMD devices. It was found that neglecting slip velocity and temperature jump boundary conditions leads to an underestimation of the permeate flux. In addition, many effective thermal conductivity and tortuosity model combinations overestimate or underestimate the experimental data for pure water production, while others seem to fit it better.

Keywords: effective thermal conductivity; membrane distillation; slip flow; temperature jump; tortuosity

1. Introduction

Membrane distillation (MD) has been widely studied as a new technique used in desalination and water treatment. The vapor pressure gradient created by the temperature differential between the membrane's two sides, and consequently between the feed and permeate liquid streams, is the driving force behind the thermal separation process of a membrane distillation unit (Kim *et al*. 2022, Prasanna *et al*. 2023, Samadi *et al*. 2023). Thus, Direct Contact Membrane Distillation (DCMD), Air Gap Membrane Distillation (AGMD), Vacuum Membrane Distillation (VMD), and Sweeping Gas Membrane Distillation (SGMD) are the four basic configurations that can be achieved by maintaining this trans-membrane vapor pressure difference (Gabor *et al*. 2015, Prasanna *et al*. 2023, Samadi *et al*. 2023, Zamaniasl 2019). The hydrophobic properties of the porous membrane in this process create the liquid-vapor equilibrium at the pore entrance, enabling only vapor to pass through the porous membrane and ensuring the process' selectivity (Nguyen *et al*. 2022, Prasanna *et al*. 2023, Samadi *et al*. 2023, Sandid *et al*. 2022).

The porous media of the hydrophobic membrane is mainly characterized by its porosity, tortuosity, and effective thermal conductivity, which are crucial to having a better theoretical assessment of pure water production and thermal efficiency calculations (Chang *et al*. 2020).

*Corresponding author, Assistant Professor,
E-mail: loussif.nizare@gmail.com

In fact, many models are considered in membrane distillation theoretical studies to calculate the effective thermal conductivity and tortuosity (Chang *et al*. 2020, Ismail *et al*. 2021, Liu *et al*. 2020, Sparenberg 2021), the commonly used ones are presented in Table 1.

For the effective thermal conductivity, the isostrain model (Eq. 1) has been often utilized in theoretical calculations of the effective thermal conductivity of porous membranes for simulating MD processes. This model indicates an upper limit of the effective conductivity and assumes that the membrane's solid and fluid phases are parallel to the heat flux (Anqi *et al*. 2019, Chang *et al*. 2020, Liu *et al*. 2020, Zuo *et al*. 2014). The isostress model (Eq. 2), which places the fluid and solid phases perpendicular to the direction of the heat flux, is also frequently employed for the calculation of the effective thermal conductivity. The Maxwell type I model (Eq. 3) may estimate the effective thermal conductivity if the membrane structure is considered to be represented by inclusions of randomly dispersed and non-interacting spherical solid particles spread in the fluid phase (Garcia-Payo *et al*. 2004, Hitsov *et al*. 2015, Srisurichan *et al*. 2006, Sparenberg *et al*. 2021).

On the other side, for tortuosity models, the Bruggemman's correlation for porous media with randomly distributed pores inside a solid matrix characterized by obstacles in the cylindrical or spherical format, respectively, may be used to construct the fractal approach for tortuosity models given by Eqs. (4) and (5) (Hitsov *et al*. 2015, Huang and Reprogle 2018, Ismail *et al*. 2021). The porous system represented by an ordered cubic porous lattice provides the basis for the

ISSN: 2005-8624 (Print), 2092-7037 (Online)

Table 1 Effective thermal conductivity (k_e) and tortuosity (τ) models

Effective thermal conductivity (k_e) models	Ref.	Eq.
$k_e = (1-\varepsilon)k_m + \varepsilon k_v$	Chang *et al*. 2020 Lu *et al*. 2019	(1)
$k_e = \left(\frac{\varepsilon}{k_v} + \frac{1-\varepsilon}{k_m}\right)^{-1}$	Histov *et al*. 2015 García *et al*. 2004	(2)
$k_e = k_v \left(\frac{1 + 2(1-\epsilon)\frac{k_m - k_v}{k_m + 2k_v}}{1 - (1-\epsilon)\frac{k_m - k_v}{k_m + 2k_v}} \right)$	Histov *et al*. 2015 Gonzo 2002	(3)
Tortuosity (τ) models		
$\tau = \frac{1}{\epsilon}$	Ismail *et al*. 2021 Huang *et al*. 2018	(4)
$\tau = \frac{1}{\sqrt{\epsilon}}$	Ismail *et al*. 2021 Hitsov *et al*. 2015	(5)
$\tau = \frac{(2-\varepsilon)^2}{\epsilon}$	Mackie *et al*. 1995 Iversen *et al*. 1997	(6)
$\tau = \frac{\epsilon}{1-(1-\varepsilon)^{1/3}}$	Beeckman 1990 Kim 2014	(7)
$\tau = \frac{2-\varepsilon}{\epsilon}$	Tjaden *et al*. 2016	(8)
$\tau = \varepsilon^{1-\frac{D_T}{2-D_T}}$	Liu and Nie 2001 Xiao *et al*. 2019	(9)

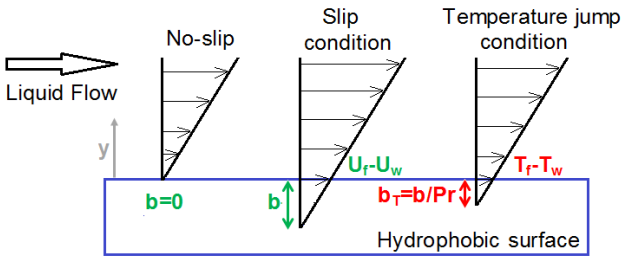

Fig. 1 Schematic representation of no-slip, slip and temperature jump conditions

tortuosity model given by Eq. (6), which is based on Euclidean geometry. In addition, the model described by Eq. (7) was developed by Beeckman from the analytical solution of the diffusion problem in heterogeneous catalysts with randomly interconnected pores. Eq. (8) represents a model based on an ordered packed structure of spheres for tortuosity calculation (Tjaden *et al*. 2016), while Eq. (9) describes a model created by Liu and Nie (2001), where the fractal dimension, D_T, and the corresponding micropore area fractal dimension may be found in Xiao *et al*. (2019).

It's obvious that tortuosity and effective thermal conductivity are interrelated, and it's important to study all combinations to find the suitable models for different membranes used in MD units.

On the other side, when modeling a desalination membrane distillation unit, the non-slip boundary condition is always used at the hydrophobic side of the membrane, but when a surface is coated with a hydrophobic substance, the fluid nearby does not adhere to the solid boundary, resulting in an overall slip velocity. This slip velocity is proportional to the fluid's normal velocity gradient near the wall with a slip length b, which may be thought of as the imaginary distance within the solid where the velocity extrapolates to zero. Slip velocity can be presented in the following form (Guan *et al*. 2015, Loussif *et al*. 2013):

$$U_f - U_w = b \left.\frac{\partial U}{\partial y}\right|_{y=0} \tag{10}$$

In this relation, U_f is the velocity of fluid at the wall, U_w is the wall velocity, b is the slip length and y is the coordinate normal to the solution flow.

Tretheway and Meinhart (2002, 2004) demonstrated experimentally an apparent fluid slip in micro-channels with hydrophobic walls. They measured the apparent slip velocity at the wall of a microchannel coated with hydrophobic octadecyltrichlorosilane. The slip velocity at the wall was 10 percent of the free stream velocity, resulting in a slip length equal to 1μm.

Furthermore, a superhydrophobic surface can significantly reduce hydrodynamic resistance, and Ou and Rothstein (2005) measured a slip length greater than 25 μm. Minghui *et al*. (2023) recorded a slip length of 165 μm, while Choi and Kim (2006) and Lee *et al*. (2008) reported slip lengths exceeding 185 μm. Moreover, due to the presence of hydrophobic/superhydrophobic surface, the temperature of the fluid particle adjacent to the wall is different from the temperature of the wall. This temperature jump is determined by a thermally equivalent interfacial thermal resistance known as Kapitza resistance (Bocquet *et al*. 2007, Karniadakis *et al*. 2005, Roy *et al*. 2013). In analogy with slip velocity, the temperature jump can be expressed as:

$$T_f - T_w = b_T \left.\frac{\partial T}{\partial y}\right|_{y=0} \tag{11}$$

where T_f indicates the fluid temperature at the wall and T_W is the wall temperature. b_T is the temperature jump length, also called Kapitza length, and it is a thermal resistance length at the solid-liquid interface.

Similar to the slip length, the Kapitza length can be interpreted as the distance inside the solid to which the temperature profile must be extrapolated to reach the wall temperature. For hydrophilic surface (with contact angle less than 90°), the Kapitza length is very small. But, for hydrophobic or superhydrophobic surface, the Kapitza length can be comparable to the slip length (Fig. 1).

It should be stated that Kapitza length has a relationship with slip length via Prandtl number (Pr) as (Barrat and Chioruttini 2003):

$$b_T = \frac{b}{Pr} \tag{12}$$

In addition, many experimental studies demonstrated

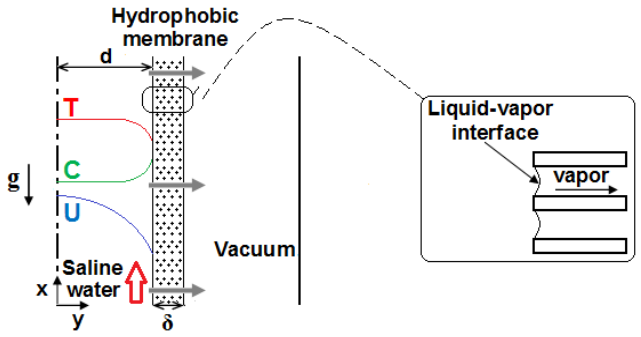

Fig. 2 Schematic diagram of the VMD unit

that slip flow and thermal jump occurred even in conventional channels coated with hydrophobic or superhydrophobic layers (Cowley *et al*. 2014, Maynes and Crockett 2014, Saadatbakhsh *et al*. 2020).

Furthermore, the majority of previous numerical studies on membrane distillation for desalination and water treatment were carried out in the no-slip regime, ignoring the impact of slip velocity brought on by the hydrophobicity of the membrane surface. Slip velocity in modeling has only been investigated in a small number of studies, while the temperature jump condition was always neglected. In addition, as mentioned in Table 1, models for tortuosity and effective thermal conductivity calculations are interrelated, and it's important to study all possible combinations to find the suitable models for membranes used in VMD.

The purpose of this study is to present a two-dimensional model for the transport phenomena in the feed channel of a VMD module used for desalination. The governing equations expressing the conservation of mass, momentum, energy and species in the hot saline solution are developed and solved numerically, as well as the mass and energy balances on the membrane sides. The slip velocity and the temperature jump boundary conditions are also considered. All possible combinations of effective thermal conductivity and tortuosity of the membrane are studied, for different MD membranes, to find suitable models.

2. Materials and methods

VMD is the configuration under consideration in this study. Fig. 2 shows a description of the physical model. Cartesian coordinates in 2D are considered. Inside a channel, a hot saline solution flows. The wall of this channel is made up of a micro porous hydrophobic membrane that allows only water vapor to permeate while retaining liquid water. A vacuum pressure is applied on the opposite side to create a partial pressure gradient, allowing vapor to diffuse across the membrane.

The conservation of mass, momentum, energy, and species in the *x* and *y* directions governs the flow, heat, and mass transfer within the hot feed saline water.

The equations in the hot saline solution domain are:

$$\frac{\partial U}{\partial x}+\frac{\partial V}{\partial y}=0 \tag{13}$$

$$U\frac{\partial U}{\partial x}+V\frac{\partial U}{\partial y}=-\frac{1}{\rho}\frac{\partial P}{\partial x}+\upsilon\left(\frac{\partial^2 U}{\partial x^2}+\frac{\partial^2 U}{\partial y^2}\right) \tag{14}$$

$$U\frac{\partial V}{\partial x}+V\frac{\partial V}{\partial y}=-\frac{1}{\rho}\frac{\partial P}{\partial y}+\upsilon\left(\frac{\partial^2 V}{\partial x^2}+\frac{\partial^2 V}{\partial y^2}\right) \tag{15}$$

$$U\frac{\partial T}{\partial x}+V\frac{\partial T}{\partial y}=\frac{k}{\rho.C_P}\left(\frac{\partial^2 T}{\partial x^2}+\frac{\partial^2 T}{\partial y^2}\right) \tag{16}$$

$$U\frac{\partial C}{\partial x}+V\frac{\partial C}{\partial y}=D\left(\frac{\partial^2 C}{\partial x^2}+\frac{\partial^2 C}{\partial y^2}\right) \tag{17}$$

The boundary conditions are:

- Inlet of the saline solution (*x=0*)

$$U=U_{in}\ ,\ V=0\ ,\ T=T_{in}\ ,\ C=C_{in} \tag{18}$$

- Symmetry conditions (*y=0*)

$$\frac{\partial U}{\partial y}=0\ ,\frac{\partial T}{\partial y}=0\ ,\frac{\partial C}{\partial y}=0\ ,V=0 \tag{19}$$

- Outlet of the saline solution (*x=L*)

$$\frac{\partial U}{\partial x}=0\ ,\frac{\partial V}{\partial x}=0\ ,\frac{\partial T}{\partial x}=0\ ,\frac{\partial C}{\partial x}=0 \tag{20}$$

- Feed saline solution - membrane interface (*y=d*)

Due to hydrophobic membrane characteristics, slip velocity and temperature jump in the feed saline solution-membrane interface are expressed as:

$$U=b\frac{\partial U}{\partial y} \tag{12}$$

$$T-T_{hm}=b_T\frac{\partial T}{\partial y} \tag{22}$$

where b and b_T are the slip length and the temperature jump length respectively.

So, the non-slip boundary condition will refers to a slip length b equal to zero, and consequently, there will be no temperature jump.

$$V=\frac{J_v}{\rho},\qquad \frac{\partial T}{\partial y}=-\frac{Q_c+Q_L}{k},\qquad \frac{\partial C}{\partial y}=\frac{J_v}{\rho D} \tag{23}$$

where $Q_L=J_v h_{fg}$ represents the latent heat flux and Q_c the conduction heat flux.

$$Q_c=\frac{T_{hm}-T_{vc}}{R_{ma}} \tag{24}$$

where T_{hm} is the temperature at the feed side membrane surface, T_{vc} is the temperature at the permeate side membrane surface and R_{ma} is the thermal resistance of the membrane defined as:

$$R_{ma}=\frac{R_m R_v}{R_m+R_v} \tag{25}$$

where the heat transfer resistance of the solid part of the membrane is:

Table 2 Influence of grid size on the pure water production

Nx,Ny		1000,50	1100,50	1000,60	1100,60
J [kg/m²h]	b=0	14.4635	14.4624	14.4620	14.4633
	b=100 μm	15.2939	15.2915	15.2924	15.2933

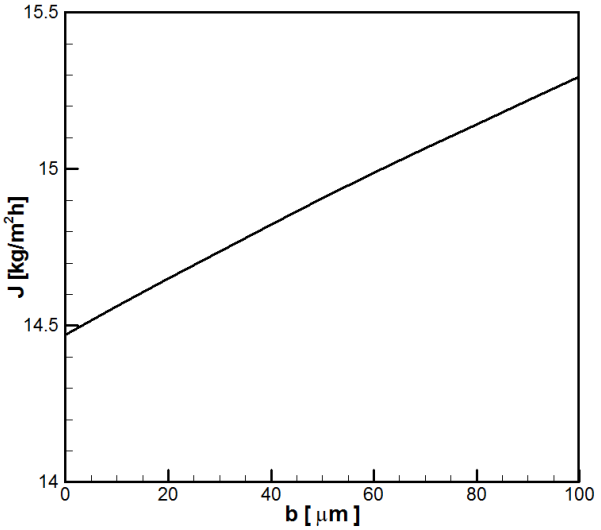

Fig. 3 Effect of slip velocity and temperature jump boundary conditions on pure water production *J*

$$R_{ma} = \frac{\delta}{k_e} \tag{26}$$

The heat transfer resistance of the vapor flow through the membrane pores is:

$$R_v = \frac{1}{J_v + Cp_v} \tag{27}$$

- Membrane-permeate flux interface (y=d+δ)

$$P = P_{vc} \tag{28}$$

where P_{vc} represents the permeate side vacuum pressure.

The local vapor flux generated by the membrane J_v, which is dependent on the membrane characteristics and the established driving force, can be expressed as (Chang *et al*. 2020, Loussif and Orfi 2014):

$$J_v = K(P_{hm} - P_{vc}) \tag{29}$$

where K is the permeability of the membrane, P_{hm} is the water vapor pressure at the feed side membrane surface and P_{vc} is the vacuum pressure at the permeate side membrane surface.

The vapor pressure P_v can be calculated using the Antoine's equation (Suleman *et al*. 2020, Loussif and Orfi 2018):

$$P_v = exp\left(23.1964 - \frac{3816.44}{T - 46.13}\right) \tag{30}$$

The effect of salt's presence on the vapor pressure at the hot surface of the membrane side has been considered and the Raoult's Law is used. So that, the vapor pressure at the hot saline solution-membrane interface P_{hm} is expressed as:

$$P_{hm} = (1 - C_M)P_v \tag{31}$$

where C_M is the mole fraction of NaCl and P_v is the vapor pressure calculated used Antoine's equation at the temperature of the hot saline-membrane interface.

The membrane permeability K is defined as (Chang *et al*. 2020):

$$K = 1.064\frac{\varepsilon . r_p}{\tau . \delta}\left(\frac{M}{R.T}\right)^{0.5} \tag{32}$$

where ε is the porosity of the membrane, τ is the tortuosity of the pores, δ is the membrane thickness, r_p is the membrane mean pore size, M is the Molar mass of water vapor, R is universal gas constant, and T is the mean temperature of the membrane.

The averaged permeate flux is defined as:

$$J = \frac{1}{L}\int_0^L J_v(x)dx \tag{33}$$

The comparison of the different model combinations would be illustrated through the evaluation of the Relative Deviation RD_i (Eq. 34) and the Root Mean Square Error RMSE (Eq. 35), between the numerical and experimental results for pure water production.

$$RD_i = \frac{J_{numerical\_i} - J_{expermental\_i}}{J_{expermental\_i}}\ 100 \tag{34}$$

$$RMSE = \sqrt{\frac{1}{n}\sum_{i=1}^{n}\left(J_{expermental\_i} - J_{numerical\_i}\right)^2} \tag{35}$$

3. Results and discussion

3.1 Numerical method

The governing equations with the boundary conditions are solved numerically using the finite volume method and the Simpler Algorithm (Versteeg *et al*. 2007). A grid-dependence analysis of the method of solution was performed as mentioned in Table 2. Based on a grid dependence analysis, the values are practically independent of the chosen grid, so we select the grid size of 1000,50 for the simulations conducted in the present investigation.

3.2 Effect of slip velocity and temperature jump

It's important to begin this study by investigating the effect of incorporating the slip velocity and temperature jump boundary conditions in modeling the VMD configuration. Fig. 3 shows the evolution of the pure water production for different slip length values. One can see that considering slip velocity and temperature jump boundary conditions increases the evaporation mass flux. In addition, the evolution of saline solution-membrane interface temperature (T_{hm}) along the normalized axial coordinate

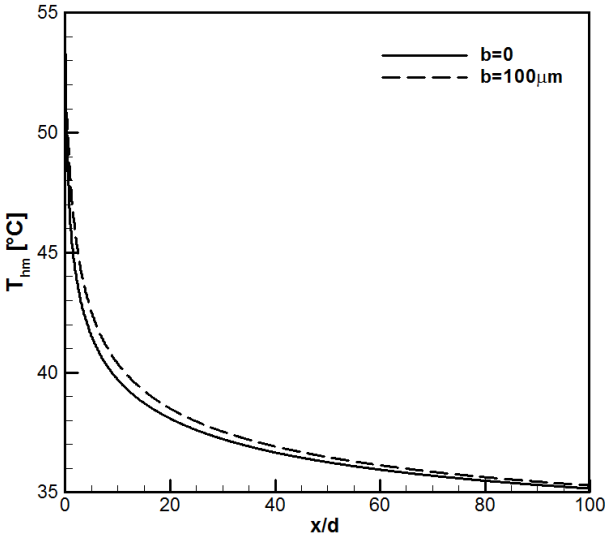

Fig. 4 Evolution of the saline solution-membrane interface temperature along the VMD device

Table 3 Specifications and operating conditions of tested membranes

Membrane	PVDF (Kim *et al*. 2021)	PTFE (Kim *et al*. 2021)	PP (Safavi and Tora 2009)
Nominal pore size (μm)	0.22	0.45	0.2
Thickness (μm)	125	89	163
Porosity (%)	75	72	75
Salt concentration (g/kg)	0-60	0-60	100-300
Temperature (°C)	60.3-61.3	59.5-61.5	25-55
Flow rate (l/min)	0.35-0.7	0.35-0.7	0.9-1.8
P_{vc} (kPa)	8-16	8-16	4-12
D (m^2/s)	2.5 10^{-9}	2.5 10^{-9}	2.5 10^{-9}
ρ (kg/m^3)	982-1026	982-1026	1057-1214
Cp (kJ/kgK)	3.90-4.18	982-1026	3.11-3.73

(*x/d*) is presented in Fig. 4. In fact, increasing the slip length *b* results in a lower temperature decrease at the saline solution-membrane interface, maintaining a larger temperature difference at the membrane sides, and producing more pure water.

Furthermore, the effect of slip length and temperature jump boundary conditions is significant even for hydrophobic membranes and becomes more pronounced for superhydrophobic surfaces (Fig. 3). Thus, it's important to integrate these boundary conditions for a rigorous VMD modeling, while neglecting them leads to an underestimation of the permeate flux.

3.3 Tortuosity and effective thermal conductivity modeling

In this section, a comparison between different combinations of tortuosity (Eqs. 1-3) and effective thermal conductivity (Eqs. 4-9) models will be conducted for commonly used VMD flat membranes under different operating conditions. Thus, experimental data from the literature will be compared to the simulation results brought by our developed model. So, different flat membrane materials will be considered (PVDF, PTFE, and PP) in a VMD device in order to select the best model combinations

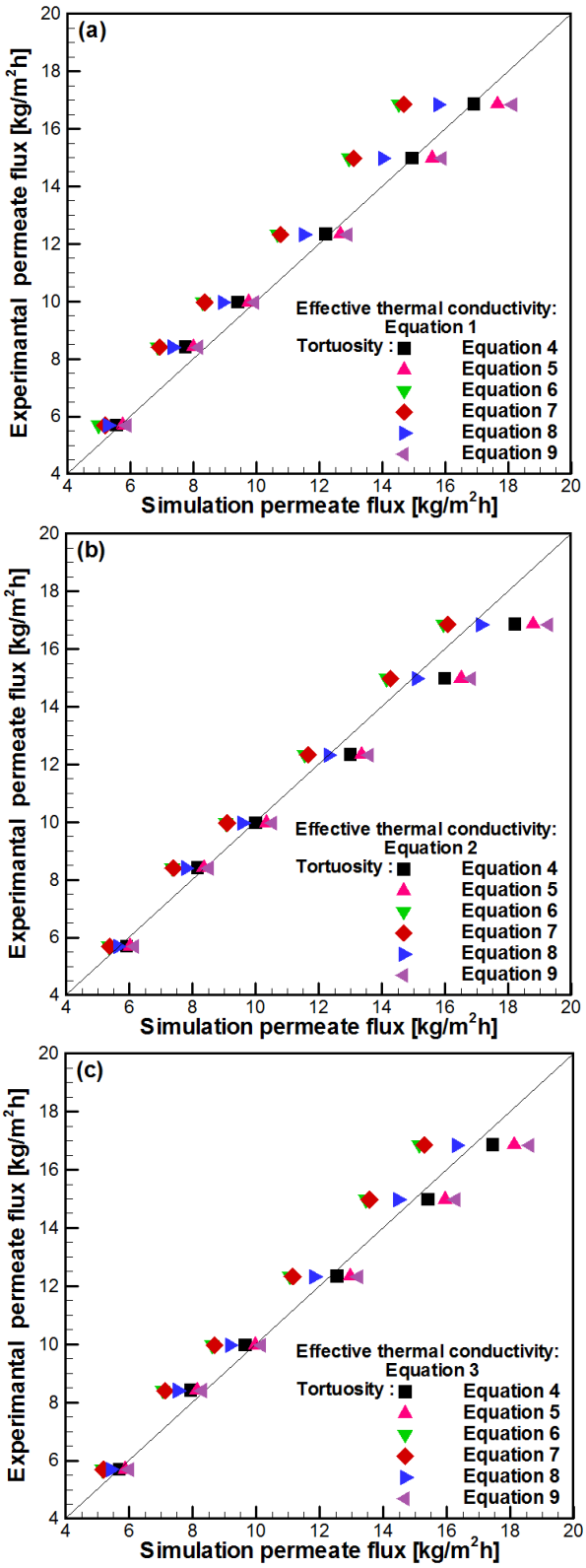

Fig. 5 Experimental versus theoretical permeate flux produced by the PVDF membrane, for all tortuosity and effective thermal conductivity model combinations

Table 4 Relative deviation (%) for the PVDF membrane module using all possible combinations of effective thermal conductivity and tortuosity models

Experimental data by Kim *et al.* (2021)				9,97	16,85	14,97	12,33	8,41	5,69
Relative deviation RD (%)	Effective thermal conductivity model	Eq 1	Tortuosity model	Eq 4	-5.62	0.36	-0.20	-0.24	-6.06	-2.28
				Eq 5	-2.31	4.69	4.01	2.60	-4.88	0.88
				Eq 6	-16.75	-13.83	-13.63	-13.46	-18.55	-12.65
				Eq 7	-16.25	-12.88	-12.56	-12.65	-17.72	-8.61
				Eq 8	-10.53	-6.47	-6.41	-6.73	-12.84	-7.21
				Eq 9	-0.20	7.66	6.28	4.70	-2.73	3.51
		Eq 2		Eq 4	0.30	8.07	6.81	5.43	-2.97	4.04
				Eq 5	3.61	11.51	8.88	8.27	-0.71	5.80
				Eq 6	-9.23	-5.34	-5.54	-6.24	-12.49	-5.98
				Eq 7	-8.73	-4.57	-4.68	-5.43	-12.01	-5.45
				Eq 8	-3.91	2.08	1.54	0.57	-7.49	-0.88
				Eq 9	5.72	14.48	12.49	10.38	1.43	8.44
		Eq 3		Eq 4	-3.11	3.56	2.94	1.78	-5.59	-0.35
				Eq 5	-0.20	7.54	6.55	5.11	-3.33	3.16
				Eq 6	-13.64	-10.21	-10.22	-10.38	-16.17	-9.49
				Eq 7	-12.84	-9.26	-9.35	-9.57	-15.10	-8.61
				Eq 8	-8.02	-3.26	-3.41	-4.14	-10.58	-4.57
				Eq 9	2.11	10.50	8.82	7.22	-1.19	5.80

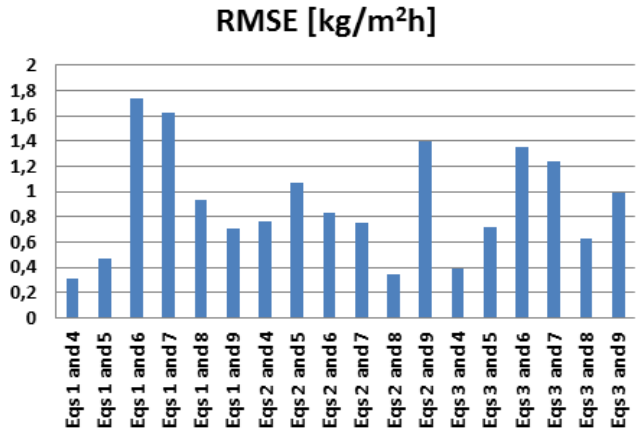

Fig. 6 RMSE between simulated permeate flux and experimental data for the PVDF membrane for all possible tortuosity and effective thermal conductivity model combinations

to fit the experimental data for the permeate flux prediction.

The specifications of the PVDF, PTFE and PP membranes and the operating conditions are shown in Table 3.

Fig. 5 shows comparisons of the theoretical pure water production results and the experimental findings of Kim *et al.* (2021) for the PVDF flat membrane. All combinations of the three effective thermal conductivity and the five tortuosity models are presented. One can see that combinations made by Eqs. (1) and (4), Eqs. (2) and (8), and Eqs. (3) and (4) seem to fit the experimental data, while the other combinations bring theoretical pure water production greater or lower than the experimental data.

In addition, from Table 4 one can see that Eqs. (1) and (4), Eqs. (2) and (8), and Eqs. (3) and (4) have a maximum relative deviation equal to -6.06%, -7.49%, and -5.59%, respectively, while the other combinations, such as Eqs. (1) and (6) and Eqs. (1) and (7) reached higher relative deviation equal to -18.54% and -17.71%, respectively.

To pick the best models from the different combinations, a statistical evaluation should be done through the global Root Mean Square Error (RMSE) between the numerical and experimental data. The results of the statistical investigation, as presented in Fig. 6, show that the models described by Eqs. (1) and (4) have the lowest RMSE of 0.3151 kg/m^{2}h, so that Eqs. (1) and (4) are the models to give the best prediction of experimental data. On the other side, Eqs. (1) and (6) have the highest RMSE of 1.7362 kg/m^{2}h which represents a remarkable difference between numerical predictions and experimental values. In addition, effective thermal conductivity and tortuosity model combinations described by Eqs. (2) and (8) and Eqs. (3) and (4) produced low RMSE values equal to 0.3492 kg/m^{2}h and 0.3914 kg/m^{2}h, respectively. So, the isostrain model given by Eq. (1) for modeling the effective thermal conductivity of the membrane and the Bruggemman's correlation for porous media with randomly distributed pores inside a solid matrix characterized by obstacles in the cylindrical format given by Eq. (4) to model tortuosity represent the best choice for modeling a PVDF flat membrane used for desalination.

The investigation of the best models for PTFE membrane that fit experimental data provided by Kim *et al.* (2021), is presented in Fig. 7. One can see that combinations made by Eqs. (1) and (4), Eqs. (2) and (7), and Eqs. (3) and (8) are in good agreement with the experimental data, while the other

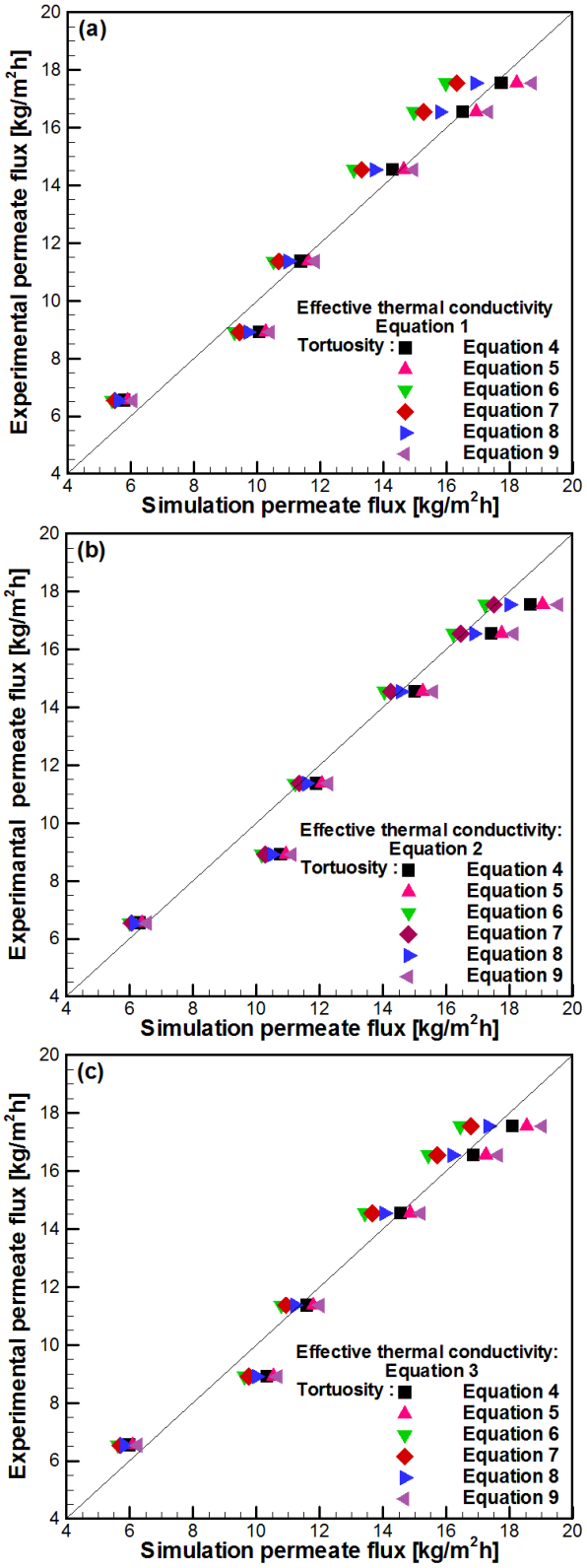

Fig. 7 Experimental versus theoretical permeate flux produced by the PTFE membrane, for all tortuosity and effective thermal conductivity model combinations

combinations remarkably overestimate or underestimate the experimental permeate flux. Table 5 also shows that the relative deviations for Eqs. (1) and (4), Eqs. (2) and (7), and Eqs. (3) and (8) are respectively, 12.96%, 15.51%, and

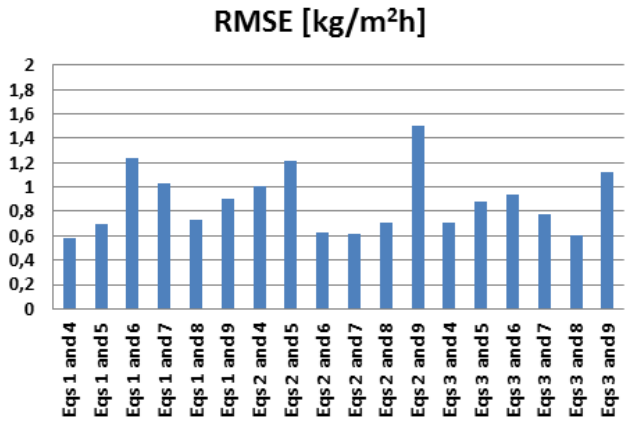

Fig. 8 RMSE between simulated permeate flux and experimental data for the PTFE membrane for all possible tortuosity and effective thermal conductivity model combinations

12.34%, while higher relative deviations for other combinations, such as Eqs. (2) and (5) and (2) and (9), are respectively, 22.71% and 25.06%.

The results of the RMSE presented in Fig. 8, show that the models described by Eqs. (1) and (4) provide the lowest RMSE of 0.5750 kg/m²h, while Eqs. (2) and (9) have the highest RMSE of 1.5005 kg/m²h.

On the other side, effective thermal conductivity and tortuosity model combinations described by Eqs. (3) and (8), Eqs. (2) and (7) and Eqs. (2) and (6) generated low RMSE values equal to 0.5981 kg/m²h, 0.6107 kg/m²h, and 0.6255 kg/m²h, respectively. Thus, the parallel model given by Eq. (1) for modeling the effective thermal conductivity of the membrane and the model based on a fractal approach given by Eq. (4) for tortuosity modeling could be adopted for a PTFE flat membrane used for desalination.

Fig. 9 depicts the analysis of the best models for PP membrane that fit experimental data reported by Safavi and Tora (2009). Combinations resulting from Eqs. (1) and (4), Eqs. (2) and (8), and Eqs. (3) and (8) are in good agreement with the experimental data, but the other combinations significantly overestimate or underestimate the experimental permeate.

Furthermore, Table 6 shows that Eqs. (1) and (4), Eqs. (2) and (8), and Eqs. (3) and (8) have a relative deviation of 3.22%, 7.93%, and -7.16%, respectively, while other combinations, such as Eqs. (1) and (6) and Eqs. (2) and (9) have a relative deviation of -21.79% and 21.96%, respectively.

Fig. 10 shows that the models given by Eqs. (1) and (4) have the lowest *RMSE* of 0.2326 kg/m²h, whereas Eqs. (2) and (9) have the highest *RMSE* of 1.9417 kg/m²h. In addition, effective thermal conductivity and tortuosity model combinations described by Eqs. (2) and (8), Eqs. (3) and (7) and Eqs. (3) and (4) produced low RMSE values of 0.3659 kg/m²h, 0.4717 kg/m²h, and 0.4903 kg/m²h, respectively.

The model given by Eq. (1) for modeling the effective thermal conductivity of the membrane and the model based on a fractal approach given by Eq. (4) for tortuosity modeling could be used for the modeling of the *PP* flat membrane used for desalination.

Table 5 Relative deviation (%) for the PTFE membrane module using all possible combinations of effective thermal conductivity and tortuosity models

Experimental data by Kim *et al.* (2021)				16.52	14.53	11.36	17.54	6.57	8.9
Relative deviation RD (%)	Effective thermal conductivity model	Eq 1	Tortuosity model	Eq 4	-0.19	-1.71	0.29	1.09	-11.33	12.96
				Eq 5	2.36	0.58	2.38	3.86	-9.79	15.28
				Eq 6	-9.52	-10.20	-7.54	-8.92	-17.26	4.23
				Eq 7	-7.65	-8.49	-5.94	-6.92	-16.04	6.01
				Eq 8	-4.53	-5.64	-3.31	-3.58	-14.04	8.93
				Eq 9	4.78	2.92	4.23	6.71	-7.03	16.96
		Eq 2		Eq 4	5.33	3.21	4.74	6.37	-3.70	20.95
				Eq 5	7.26	4.94	6.29	8.56	-2.51	22.71
				Eq 6	-1.98	-3.37	-1.26	-1.82	-8.38	14.10
				Eq 7	-0.50	-2.02	-0.02	-0.16	-7.40	15.51
				Eq 8	1.96	0.20	2.01	2.59	-5.83	17.82
				Eq 9	9.68	7.22	8.13	11.41	0.24	25.06
		Eq 3		Eq 4	1.92	0.18	4.74	3.12	-8.38	16.03
				Eq 5	4.24	2.26	3.89	5.67	-6.97	18.15
				Eq 6	-6.68	-7.61	-5.15	-6.23	-13.87	7.98
				Eq 7	-4.95	-6.03	-3.69	-4.36	-12.74	9.63
				Eq 8	-2.07	-3.42	-1.28	-1.23	-10.89	12.34
				Eq 9	6.66	4.54	5.74	8.52	-4.22	19.83

Table 6 Relative deviation (%) for the PP membrane module using all possible combinations of effective thermal conductivity and tortuosity models

Experimental data by Safavi and Tora (2009)				14.43	12.2	9.41	8.47	4.7	6.69
Relative deviation RD (%)	Effective thermal conductivity model	Eq 1	Tortuosity model	Eq 4	0.27	-3.88	-1.48	1.99	1.42	3.22
				Eq 5	6.59	1.83	3.66	7.04	3.54	7.87
				Eq 6	-19.31	-21.79	-17.90	-14.75	-14.44	-12.53
				Eq 7	-18.12	-20.69	-16.87	-13.69	-13.53	-11.52
				Eq 8	-9.57	-12.83	-9.53	-5.18	-7.24	-4.47
				Eq 9	9.77	4.67	6.15	9.53	5.50	10.15
		Eq 2		Eq 4	12.87	9.47	10.54	12.47	11.30	15.01
				Eq 5	18.94	14.81	15.17	17.19	14.96	19.24
				Eq 6	-6.48	-7.93	-5.11	-3.57	-1.69	0.30
				Eq 7	-5.28	-6.84	-4.10	-2.53	-0.82	1.27
				Eq 8	3.25	0.88	2.92	4.68	5.11	7.93
				Eq 9	21.96	17.45	17.43	19.48	16.70	21.28
		Eq 3		Eq 4	5.55	1.69	3.62	6.43	4.51	8.20
				Eq 5	11.79	7.26	8.52	11.36	8.41	12.71
				Eq 6	-14.01	-16.11	-12.61	-10.07	-9.10	-7.19
				Eq 7	-12.82	-15.01	-11.58	-9.01	-8.20	-6.19
				Eq 8	-4.24	-7.16	-4.34	-1.63	-2.03	0.74
				Eq 9	14.91	10.04	10.92	13.78	10.29	14.89

4. Conclusions

This paper presents and discusses a numerical model for solving the mass, momentum, energy, and species conservation equations for the feed saline solution domain of a vacuum membrane distillation device. The slip velocity and temperature jump boundary conditions were also considered due to membrane hydrophobicity. A comparison between the experimental and numerical data for a combination of the most commonly used models for

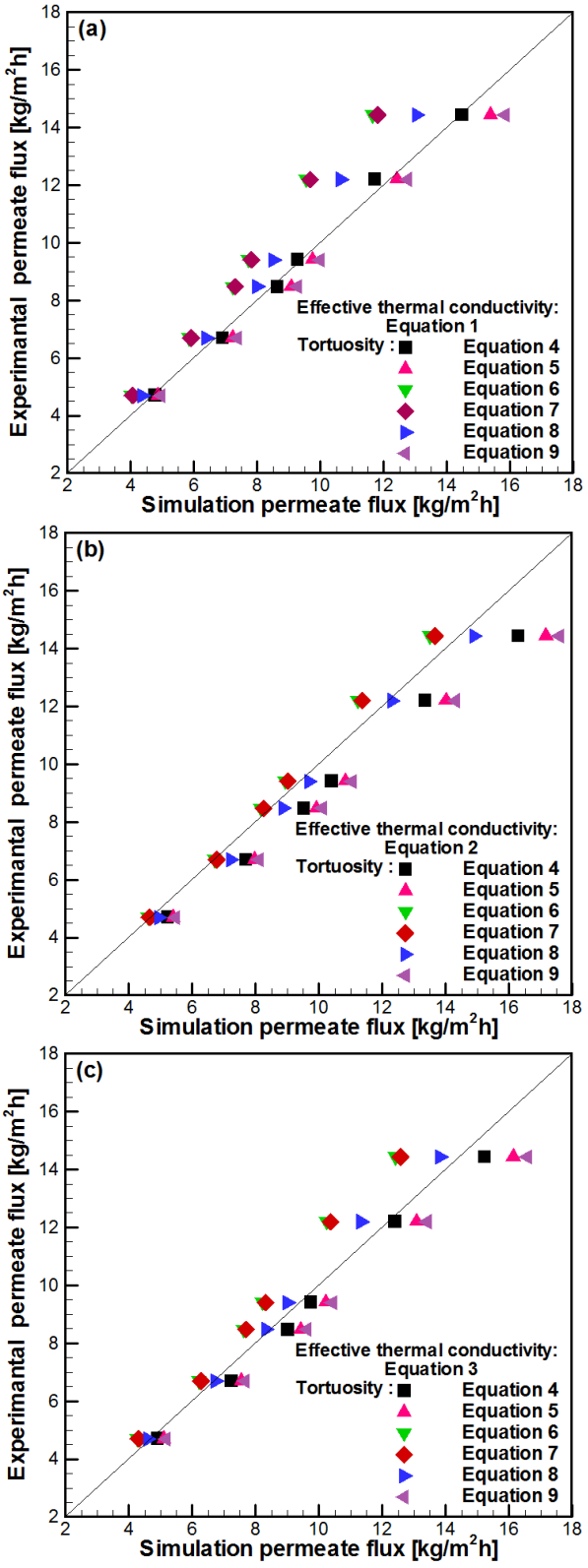

Fig. 9 Experimental versus theoretical permeate flux produced by the PP membrane, for all tortuosity and effective thermal conductivity model combinations

tortuosity and effective thermal conductivity has been conducted for different flat membrane materials (PVDF, PTFE, and PP). The influence of slip length and temperature jump boundary conditions was found to be

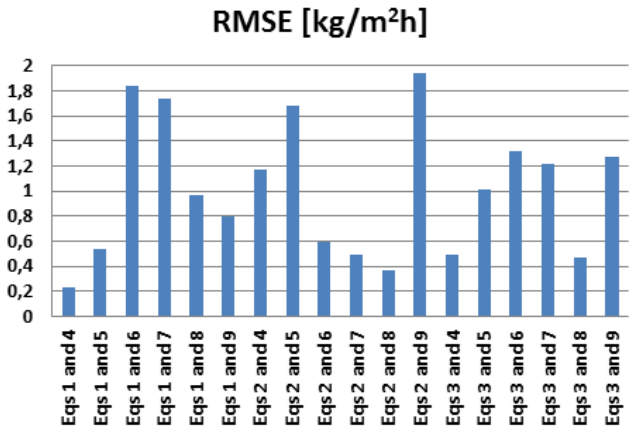

Fig. 10 RMSE between simulated permeate and experimental data for the PP flat membrane for all possible tortuosity and effective thermal conductivity model combinations

significant for hydrophobic membranes and becomes greater for superhydrophobic ones; therefore, they must be considered for rigorous VMD modeling. Also, the combination of the effective thermal conductivity and the tortuosity models described respectively by Eqs. (1) and (4) produces the best numerical fitting of the experimental data with the lowest RMSE among the other combinations for the three membrane materials, while some combinations highly overestimate or underestimate the prediction of pure water production.

References

Anqi, A.E., Usta, M., Krysko, R., Lee, J.G., Ghaffour, N. and Oztekin, A. (2019), "Numerical study of desalination by vacuum membrane distillation – Transient three-dimensional analysis", *J. Membr. Sci.*, **596**, 117609. https://doi:10.1016/j.memsci.2019.117609

Barrat J.L. and Chiaruttini, F. (2003), "Kapitza resistance at the liquid solid interface", *Mol. Phys.* **101**, 1605-1610. https://doi.org/10.1080/0026897031000068578

Beeckman, J.W. (1990), "Mathematical description of the heterogeneous materials", *Chem. Eng. Sci.*, **45**(8), 2603-2610. https://doi.org/10.1016/0009-2509(90) 80148-8.

Bocquet L. and Barrat J.L. (2007), "Flow boundary conditions from nano- to micro-scales", *Soft Matter.*, **3**, 685-693. https://doi: 10.1039/B616490K

Chang, Y.S., Ooi, B.S., Ahmad, A.L., Leo, C.P. and Lau, W.J. (2020), "Numerical study on performance and efficiency of batch submerged vacuum membrane distillation for desalination", *Chem. Eng. Res. Des.*,**163**, 217-229. https://doi.org/10.1016/j.cherd.2020.08.031

Choi, C.H. and Kim, C.J. (2006), "Large slip of aqueous liquid flow over a nanoengineered superhydrophobic surface", *Phys. Rev. Lett.*, **96**, 066001. https://doi.org/10.1103/PhysRevLett.96.066001.

Cowley, A., Maynes, D., Crockett, J. (2014), "Effective temperature jump length and influence of axial conduction for thermal transport in superhydrophobic channels", *Int. J. Heat Mass Transf.*, **79**, 573-583. https://doi.org/10.1016/j.ijheatmasstransfer.2014.08.033

Gábor R., Steffen K., Oliver S., Benjamin S., Zoltán K., Gyula V., Mehrdad E. and Peter C. (2015), "Experimental determination

of liquid entry pressure (LEP) in vacuum membrane distillation for oily wastewaters", *Membr. Water Treat.*, **6**(3), 237-249. https://doi.org/10.12989/mwt.2015.6.3.237

García-Payo, M.C. and Izquierdo-Gil M.A. (2004), "Thermal resistance technique for measuring the thermal conductivity of thin microporous membranes", *J. Phys. D. Appl. Phys.*, **37**(21) 3008-3016. https://doi.org/10.1088/0022-3727/37/21/011.

Gonzo, E.E. (2002) "Estimating correlations for the effective thermal conductivity of granular materials", *Chem. Enq. J.*, **90** 299-302. https://doi.org/10.1016/S1385-8947(02)00121-3

Guan, N., Liu, Z., Jiang, G., Zhang, C. and Ding, N. (2015), "Experimental and theoretical investigations on the flow resistance reduction and slip flow in super-hydrophobic micro tubes", *Experim. Therm. Fl. Sci.*, **69**, 45-57. https://doi.org/10.1016/j.expthermflusci.2015.08.003

Hitsov, I., Maere, T., De Sitter, K., Dotremont, C. and Nopens, I. (2015), "Modelling approaches in membrane distillation: A critical review", *Sep. Purif. Technol.*, **142**, 48-64. https://doi.org/10.1016/j.seppur.2014.12.026

Huang, F.Y.C. and Reprogle, R. (2018), "Thermal conductivity of polyvinylidene fluoride membranes for direct contact membrane distillation", *Environ. Eng. Sci.*, **36**(4). https://doi:10.1089/ees.2018.0349

Ismail, M. S., Mohamed, A. M., Poggio, D. and Pourkashanian, M. (2021). "Direct contact membrane distillation: A sensitivity analysis and an outlook on membrane effective thermal conductivity", *Journal of Membrane Science*, **624**, 119035. https://doi:10.1016/j.memsci.2020.119035

Iversen, S.B. Bhatia, V.K., Dam-Johansen, K. and Jonsson, G. (1997), "Characterization of microporous membranes for use in membrane contactors", *J. Membr. Sci.*, **130**(1-2), 205-217. https://doi.org/10.1016/S0376-7388(97)00026-4.

Karniadakis G., Beskök, A. and Aluru N. R. (2005), "Microflows and nanoflows- fundamentals and simulation", *Springer Verlag*, 29. https://doi.org/10.1007/0-387-28676-4

Kim Y., Choi J., Choi Y. and Lee S. (2022), "Effect of membrane deformation on performance of vacuum assisted air gap membrane distillation (V-AGMD)", *Membr. Water Treat.*, **13**(1), 51-62. https://doi.org/10.12989/mwt.2022.13.1.051

Kim H., Yun T., Hong S. and Lee S. (2021), "Experimental and theoretical investigation of a high performance PTFE membrane for vacuum-membrane distillation", *J. Membr. Sci.*, **617**, 118524. https://doi.org/10.1016/j.memsci.2020.118524.

Kim, A.S. (2014), "Cylindrical cell model for direct contact membrane distillation (DCMD) of densely packed hollow fibers", *J. Membr. Sci.*, **455**, 168-186. https://doi. org/10.1016/j.memsci.2013.12.067.

Lee, C., Choi, C.H. and Kim, C.J. (2008), "Structured surfaces for giant liquid slip", *Phys. Rev. Lett.*, **101**, 064501. https://doi.org/10.1103/PhysRevLett.101.064501.

Liu J.G. and Y.F. Nie, (2001), "Fractal scaling of effective diffusion coefficient of solute in porous media", *J. Environ. Sci.* **13**(2), 170-172. https://doi.org/10.1007/s11665-023-08731-6

Liu, J., Li, X., Zhang, W., Li, B. and Liu, C. (2020), "Superhydrophobic-slip surface based heat and mass transfer mechanism in vacuum membrane distillation", *J. Membr. Sci.*, 118505. https://doi.org/10.1016/j.memsci.2020.118505.

Loussif, N., Orfi, J. and Omri A. (2013), "Slip flow effect on laminar convection inside micro-tubes with permeable walls", *Desalin. Water Treat.*, 1973-1079. https://doi.org/10.1080/19443994.2012.714735

Loussif, N. and Orfi, J. (2014), "Effect of slip velocity on air gap membrane distillation process", *Membr. Water Treat.*, **5**(1), 57-71. https://doi.org/10.12989/mwt.2014.5.1.057

Loussif, N. and Orfi, J. (2018), "Heat and mass transfer in sweeping gas membrane distillation", *Desalin. Water Treat.*, **131**, 1-8. https://doi.org/10.5004/dwt.2018.22937

Lu, K.J., Cheng, Z.L., Chang, J., Luo, L. and Chung, T.S. (2019), "Design of zero liquid discharge desalination (ZLDD) systems consisting of freeze desalination, membrane distillation, and crystallization powered by green energies", *Desalination*, **458**, 66-75. https://doi.org/10.1016/j.desal.2019.02.001

Mackie, J.S. and Meares, P. (1995), "The diffusion of electrolytes in a cation-exchange resin membrane I. Theoretical", *Proceedings of the Royal Society of London. Series A. Mathematical and Physical Sciences*, **232**(1191), 498-509. https://doi.org/10.1098/rspa.1955.0234.

Maynes, D. and Crockett, J. (2014), "Apparent temperature jump and thermal transport in channels with streamwise rib and cavity featured superhydrophobic walls at constant heat flux", *J. Heat Transf.*, **136**, 011701-1. https://doi.org/10.1115/1.4025045

Minghui, G., Zhang, G., Xin, G., Huang, H., Huang, Y., Rong, Y. and Wu, C. (2023), "Laser direct writing of rose petal bio-mimetic micro-bulge structure to realize superhydrophobicity and large slip length", *Eng. Asp.*, **664**, 130972. https://doi.org/10.1016/j.colsurfa.2023.130972

Nguyen H.T., Manh Bui, H.,Wang, Y.F. and You, S.J. (2022), "Nonfluoroalkyl functionalized hydrophobic surface modifications used in membrane distillation for cheaper and more environmentally friendly applications: A mini-review", *Sust. Chem. Pharm.*, **28**, 100714. https://doi.org/10.1016/j.scp.2022.100714

Ou, J. and Rothstein, J.P. (2005), "Direct velocity measurements of the flow past drag-reducing ultrahydrophobic surfaces", *Phys. Fl.*, **17**, 103606. https://doi.org/10.1063/1.2109867.

Prasanna N.S., Choudhary, N., Singh, N. and Raghavarao, K.S.M.S. (2023), "Omniphobic membranes in membrane distillation for desalination applications: A mini-review", *Chem. Eng. J. Adv.*, **14**, 100486. https://doi.org/10.1016/j.ceja.2023.100486

Roy, P., Anand, N.K. and Banerjee, D. (2013), "Liquid slip and heat transfer in rotating rectangular microchannels", *Int. J. Heat Mass Transf.*, **62**, 184-199. https://doi.org/10.1016/j.ijheatmasstransfer.2013.02.043

Saadatbakhsh, M., Asl, S.J., Kiani, M.J., Nouri, N.M. (2020), "Slip length measurement of pdms/hydrophobic silica superhydrophobic coating for drag reduction application", *Surf. Coat. Technol.*, 126428. https://doi.org/10.1016/j.surfcoat.2020.126428

Safavi, M. and Tora, M. (2009), "High salinity desalination using VMD", *Chem. Eng. J.*, **149**, 191-195. https://doi.org/10.1016/j.cej.2008.10.021.

Samadi A., Ni, T., Fontananova, E., Tang, G., Shon, H. and Zhao, S. (2023), "Engineering antiwetting hydrophobic surfaces for membrane distillation: A review", *Desalination*, **563**, 116722. https://doi.org/10.1016/j.desal.2023.116722.

Sandid, A.M., Nehari D. and Nehari T. (2022), "Effective study of operating parameters on the membrane distillation processes using various materials for seawater desalination", *Membr. Water Treat.*, **13**(5), 235-243. https://doi.org/10.12989/mwt.2022.13.5.235.

Sparenberg, M.C., Hanot, B., Molina-Fernández, C. and Luis, P. (2021), "Experimental mass transfer comparison between vacuum and direct contact membrane distillation for the concentration of carbonate solutions", *Sep. Purif. Technol.*, **275**, 119193. https://doi.org/10.1016/j.seppur.2021.119193.

Srisurichan S., Jiraratananon R. and Fane A. (2006), "Mass transfer mechanisms and transport resistances in direct contact membrane distillation process", *J. Membr. Sci.*, **277**(1-2), 186-194. https://doi.org/10.1016/j.memsci.2005.10.028

Suleman, M., Asif, M., Asad, J.S., Pengyu, D. and Xi, X. (2020), "A numerical study on the effects of operational parameters and membrane characteristics on the performance of vacuum membrane distillation (VMD)", *Desalin. Water Treat.*, **183**, 182-193. https://doi.org/10.5004/dwt.2020.25320

Tjaden, B., Cooper, S.J. Brett, D.J. Kramer, D. and Shearing, P.R. (2016), "On the origin and application of the Bruggeman correlation for analysing transport phenomena in electrochemical systems", *Curr. Opin. Chem. Eng.*, **12**, 44-51. https://doi. org/10.1016/j.coche.2016.02.006.

Tretheway, D.C. and Meinhart, C.D. (2004), "A generating mechanism for apparent fluid slip in hydrophobic micro-channels", *Phys. Fl.*, **16**, 1509. https://doi.org/10.1063/1.1669400.

Tretheway, D.C. and Meinhart, C.D. (2002), "Apparent fluid slip at hydrophobic microchannel walls", *Physics of Fluids*, **14**, L9. https://doi.org/10.1063/1.1432696.

Versteeg, K. and Malalasekera, W. (2007), *An Introduction to Computational Fluid Dynamics: The Finite Volume Method*", (2nd edition), Pearson and Prentice Hall, London. U.K.

Xiao, B., Wang, W., Zhang, X., Long, G., Fan, J., Chen, H. and Deng, L. (2019), "A novel fractal solution for permeability and Kozeny-Carman constant of fibrous porous media made up of solid particles and porous fibers", *Powder Technol.*, **349**, 92-98. https://doi.org/10.1016/j.powtec.2019.03.028

Zamaniasl M. (2019), "Numerical study of direct contact membrane distillation process: Effects of operating parameters on TPC and thermal efficiency", *Membr. Water Treat.*, **10**(5), 387-394. https://doi.org/10.12989/mwt.2019.10.5.387

Zuo, G., Guan, G. and Wang, R. (2014), "Numerical modeling and optimization of vacuum membrane distillation module for low-cost water production", *Desalination*, **339**, 1-9. https://doi.org/10.1016/j.desal.2014.02.005

KC

Nomenclature

b	slip length [m]
b_T	temperature jump length [m]
C	mass fraction of NaCl
C_M	mole fraction of NaCl
C_p	specific heat [$Jkg^{-1}K^{-1}$]
d	half-width of the flow channel [m]
d_h	hydraulic diameter [m]
D	diffusion coefficient of NaCl [m^2/s]
h_{fg}	latent heat of evaporation [J/kg]
J	length-averaged permeate flux at the hot side of the membrane [kg/m^2h]
J_v	local permeate flux at the hot side of membrane, in vapor phase [kg/m^2s]
K	permeability of the membrane [kg/m^2sPa]
k	thermal conductivity [W/mK]
L	membrane length [m]
M	molar mass of water vapor [$kgkmol^{-1}$]
n	Number of experimental measurements
N_x	number of nodes along x direction
N_y	number of nodes along y direction
P	pressure [Pa]
P_{hm}	hot side pressure [Pa]
P_v	vapor pressure [Pa]
P_{vc}	vacuum pressure [Pa]
Pr	Prandtl number
Q_C	conductive heat flux [kJ/m^2h]
Q_L	latent heat flux [kJ/m^2h]
R	Universal gas constant [J/kmol K]
Re	Reynolds number
R_{ma}	thermal resistance of the membrane [$K\ m^2h\ /kJ$]
R_m	thermal resistance of the solid part of the membrane [$K\ m^2h\ /kJ$]
R_v	thermal resistance of the vapor flow through membrane [$K\ m^2h\ /kJ$]
r_p	membrane mean pore size [m]
T	temperature [°C]
U	axial velocity component [m/s]
V	radial velocity component [m/s]
x	coordinate along to the solution flow [m]
y	coordinate normal to the solution flow [m]
μ	dynamic viscosity [$kgm^{-1}s^{-1}$]
υ	cinematic viscosity [m^2s^{-1}]
ρ	density [kgm^{-3}]
ε	porosity
τ	tortuosity

δ	membrane thickness [m]

Subscripts

a	air
e	effective
in	inlet
hm	hot side membrane
m	membrane material
ma	membrane
v	vapor
vc	vacuum